ARTICLE NO. 78-1110

A Procedure for Optimizing the Design of Scramjet Engines

P.J. Waltrup,* F.S. Billig,† and R.D. Stockbridge‡
The John Hopkins University Applied Physics Laboratory, Laurel, Md.

Although the concept of using a supersonic combustion ramjet engine to propel a vehicle at hypersonic speeds through the atmosphere has been thoroughly established over the past two decades, and analyses for determining the performance of each of its components documented, no complete engine cycle analysis has been presented to date. The purpose of this paper is to review and discuss the individual component analyses previously developed, combine them into a unified cycle analysis, and present the methodology needed to optimize the design of a scramjet engine using the unified cycle analysis. A specific example applying this optimization procedure to a missile design is also included.

Nomenclature

A	= area
$C_{1,2}$	= constants used in Eqs. (14) and (15)
C_D	= drag coefficient
$\bar{C}_f$	= average skin friction coefficient
C_F, C_T	= net and gross thrust coefficients, respectively
D	= diameter
ER	= fuel-air equivalence ratio
f	= fuel-air ratio
$\mathfrak{F}$	= stream thrust $= pA + \rho u^2 A$
F	= thrust
g	= gravitational constant
h	= enthalpy
Δh	= enthalpy difference, Eq. (10)
ΔH_f	= lower heating value of fuel
$K_{1,2}$	= constants used in Eqs. (4) and (5)
L	= length
ΔL	= length change
M	= Mach number
M_{des}	= inlet design Mach number
p	= pressure
q	= dynamic pressure
$\dot{q}$	= heat flux per unit area
$\bar{Q}$	= average total heat flux
ΔQ_i	= inlet heat loss
r	= recovery factor
s	= entropy
T	= temperature
u	= velocity
$\dot{w}$	= mass flow rate
Z	= altitude
α	= divergence angle of combustor
β	= fuel injection angle
γ	= ratio of specific heats
ϵ	= exponent used in Eq. (16)
τ	= shear stress
ρ	= density
η_c	= combustion efficiency
$\eta_{p_t,KE,KD}$	= inlet efficiencies
η_n	= nozzle efficiency

Subscripts

0-6	= axial stations given in Fig. 1
1′	= state shown in Fig. 2
c	= combustor
d	= air duct
f	= fuel
i	= inlet
r	= recovery
t	= total or stagnation condition
w	= wall

Superscript

$(\bar{\ })$	= average value

Presented as Paper 78-1110 at the AIAA/SAE 14th Joint Propulsion Conference, Las Vegas, Nev., July 25-27, 1978; submitted Aug. 30, 1978; revision received Dec. 15, 1978.

Index categories: Airbreathing Propulsion; Combustion and Combustor Designs.

*Supervisor, Supersonic Combustion Section. Asociate Fellow AIAA.

†Assistant Supervisor, Aeronautics Division. Associate Fellow AIAA.

‡Associate Engineer, Propulsion Group. Associate Member AIAA.

Introduction

DURING the past twenty years or so a propulsion cycle based on heat release in supersonic flow has evolved from an interesting concept[1] to an engineering reality as evidenced by free jet tests of a variety of supersonic combustion ramjet engine (scramjet) designs.[2] To enable the successful development of these free jet devices, numerous tests of the engine components,[3] that is, inlets, combustors, and nozzles, have been made and the rudiments of a descriptive analysis of the complex aerothermochemical processes[4] have been established.

Now that the feasibility of scramjets has been demonstrated, it would be prudent to exploit the distinct advantages of this engine cycle for use in propulsion systems that must operate at Mach numbers M_0 greater than about 6. To enable those who must select the propulsion system for a vehicle to conduct a prescribed mission, it is necessary to have an engineering model for estimating performance. The exposition of an analytical model used extensively in composite design and mission analysis studies at JHU/APL will be described herein. This will include the presentation of a procedure to optimize engine performance in accordance with particular design constraints.

Engine Cycle Analysis

It is convenient to subdivide the scramjet engine process into the flow regions shown in Fig. 1. Conceptually, each of the components (inlet, thru-duct isolator, combustor, and nozzle) is analyzed separately and some combination of experimental data and analytical modeling is inherent in the analysis of each component. In general, an integral approach is used, that is, convenient control volumes are defined such that a one-dimensional representation of the flow at each of

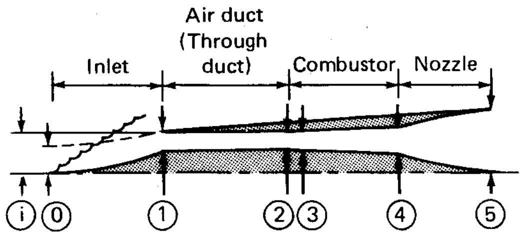

Fig. 1 Schematic of typical scramjet engine.

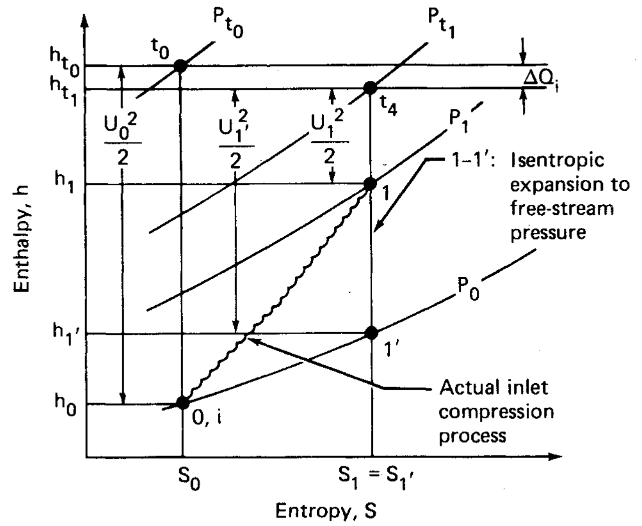

Fig. 2 Enthalpy-entropy diagram of inlet compression process.

the major stations (viz., 1-5) can be made and the details of the processes between stations are handled in a "global" manner. The intent is to simplify the analysis of representing the flow at each of the stations by the most appropriate set of one-dimensional properties. The far more rigorous analysis where the unidimensional representation is relaxed, e.g., shock-characteristics solutions of the inlet and thru-duct inviscid flowfields, streamtube analysis[5] of the combustor or finite-difference analysis[6] of the combustor-nozzle, etc., are also made, but only to provide a basis for either defining or checking the adequacy of the one-dimensional method.

Inlet

Figure 2 is an enthalpy h vs entropy s diagram of the inlet compression process with a grid of selected isobars. Conditions at point 0 correspond to the undisturbed freestream, and at point 1 to the end of inlet compression. Point 1′ corresponds to the final state of a hypothetical isentropic expansion from $p=p_l$ to $p=p_0$ at $s=s_l=s_l'$. Properties at the corresponding stagnation conditions have a prefix subscript t. The heat loss in the inlet process is $\Delta Q_i = h_{t_0} - h_{t_l}$. Three inlet efficiencies are defined:

$$\text{Total pressure efficiency} \quad \equiv \eta_{p_t} = p_{t_l}/p_{t_0} \tag{1}$$

$$\text{Kinetic energy efficiency} \quad \equiv \eta_{KE} = u_l'^2/u_0^2 = (h_{t_l} - h_l')/(h_{t_0} - h_0) \tag{2}$$

$$\text{Process efficiency} \equiv \eta_{KD} = (h_l - h_l')/(h_l - h_0) \tag{3}$$

Conditions at 0 relating p_0 and T_0 with altitude Z are based on the ICAO standard atmosphere.[7] Properties of the fluid at a point are obtained from a defined set of atomic mass fractions by determining the chemical composition, assuming thermochemical equilibrium, using curve fits of JANAF thermochemical data.[8] The air is assumed to be composed of 0.75529 nitrogen, 0.23145 oxygen, and 0.01326 argon by mass. The equilibrium calculation (identified herein as NOTS), which accounts for dissociation of the air and/or fuel combustion product species present, is based on Ref. 9.

Heat loss in the inlet is handled quite simply, i.e., for an uncooled flight-type inlet in-flight or in a freejet test, the primary loss is by radiation and

$$\Delta Q_i \approx K_l (\bar{T}_w^4 - T_0^4) \tag{4}$$

where the value of K_l is determined for a particular inlet configuration with consideration given to the exposed surface area, view factor, and emissivity. Either a constant value for $\bar{T}_w$ is assumed or a simplified dependence on M_0 and Z. For wind-tunnel or freejet model tests, the inlet surfaces are generally cool, radiation is insignificant, but heat sink losses can be important. Here,

$$\Delta Q_i \approx K_2 (T_{t_0} - \bar{T}_w) \tag{5}$$

where the values for K_2 and $\bar{T}_w$ are obtained from either a boundary-layer heat transfer calculation or from an experimental correlation.[10]

Inlet calculations can be made for nine possible combinations by specifying A_l/A_0, p_l/p_0 or M_l and η_{p_t}, η_{KE} or η_{KD}. Generally, for performance calculations the inlet geometric contraction ratio A_i/A_l is specified and the inlet air capture ratio A_0/A_i and one of the efficiencies are defined as a function of M_0. The energy and continuity equations are then solved simultaneously to obtain properties at station 1.

Thru-Duct Isolator

The thru-duct isolator calculation is performed as a degenerate case of the combustor which is discussed later. That is, the calculation corresponds to equivalence ratio, ER = 0 and frictional, shock-free flow for a defined exit-to-inlet area ratio.

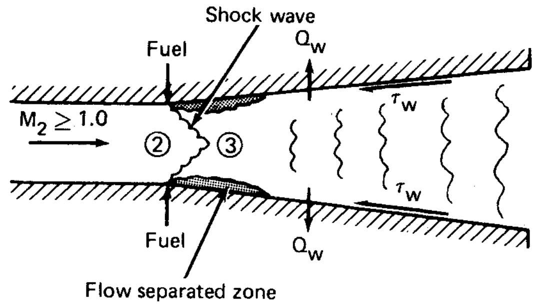

Fig. 3 Schematic of supersonic combustion process.

Combustor

Figure 3 depicts the model used to analyze the combustor. Stations 2 and 4 correspond to the entrance and exit of the combustor, respectively. As before, the flow is assumed unidimensional at these stations. Station 3 corresponds to conditions that would exist behind a single compression wave with upstream properties of station 2. The strength of the wave varies from a Mach wave, i.e., no shock, through the complete family of oblique shocks to a maximum of a normal shock.[4] For the cases of no shock or normal shock $A_3 = A_2$, but for oblique shocks the effective cross-sectional area of the flow does not correspond to a physical cross section (e.g., when the flow is separated) of the combustor, as it need not in an integral analysis. Flow through the combustor is calculated by solving simultaneously the appropriate conservation equations which are

Mass:

$$g\rho_2 u_2 A_2 + \dot{w}_f = g\rho_4 u_4 A_4 \tag{6}$$

Momentum (axial):

$$p_2A_2+\int_2^4 p_w \sin\alpha \, dA_w - p_4A_4 - \int_2^4 \tau_w \cos\alpha \, dA_w$$
$$+p_fA_f\cos\beta = \rho_4u_4^2A_4-\rho_2u_2^2A_2-\rho_fu_f^2A_f\cos\beta \qquad (7)$$

Energy:

$$h_2+\frac{u_2^2}{2}+f\left(h_f+\frac{u_f^2}{2}\right)=(1+f)\left(h_4+\frac{u_4^2}{2}\right)+\frac{1}{\dot{w}_2}\int_2^4 \dot{q}_w dA_w \qquad (8)$$

To obtain solutions to these equations, it is necessary to have both an appropriate equation of state, that is,

$$p_4=p_4(\rho_4,h_4) \qquad (9)$$

and expressions for the wall distribution of pressure, shear, and heat transfer. For the state relationship, thermodynamic equilibrium is assumed and NOTS is used with the previously defined chemical composition for air and a suitable description of the atomic mass fractions of the fuel. In the event that a calculation is being made for a case of combustion efficiency <1, the method usually followed is to assume an $ER_{eff}=ER_{actual}\cdot\eta_c$ and to neglect the mass of an equivalent weight of fuel $(1-\eta_c)\dot{w}_{f_{actual}}$ in Eqs. (6-8). For more rigorous calculations, the actual fuel flow rate is used and pseudoequilibrium between unreacted fuel and products of combustion in thermodynamic equilibrium at the local temperature and pressure is assumed for the determination of state properties at station 4.

The integral terms for the skin friction and heat transfer in Eqs. (7) and (8) for these types of flows can be obtained either by rigorous solutions of the boundary-layer equations[11] or from data correlations. At present, using data correlations is not only vastly simpler but probably more accurate. Figure 4 shows the heat flux and shear parameters that have been adopted. They are based on correlations of experimental data from a variety of fuels and combustor geometries over a wide range of initial conditions. The average heat transfer rate per unit surface area, $\bar{Q}/A_w$, is normalized by the inlet mass flux, $\dot{w}_2/A_2$, and the average gas-wall enthalpy difference defined as

$$\Delta h = h_{t_2}+f\cdot h_{t_f}+0.5\cdot f\cdot\eta_c\cdot\Delta H_f-\bar{h}_w \qquad (10)$$

where h_{t_f} is the total enthalpy of the fuel and $\bar{h}_w$ is the enthalpy of air at the average wall temperature. The factor of 0.5 multiplying the heat release parameter $f\cdot\eta_c\cdot\Delta H_f$ is intended to yield an average for the overall combustor. Thus, values of $(\bar{Q}/A_w)/(\dot{w}_a\Delta h/A_2)$ from Fig. 4 for a given heat release $f\cdot\Delta H_f\cdot\eta_c$ are multiplied by $\Delta hA_w/A_2$ to obtain the last term in Eq. (8).

Assuming that the Reynolds analogy is valid for flow with exothermic reactions, it is possible to relate the heat transfer parameter to a shear stress parameter $\bar{C}_f$. To obtain the deduced shearing stress using Reynolds analogy, certain simplifying assumptions are necessary. The analogy is expressed as

$$\frac{\bar{Q}/A_w}{\bar{h}_r-\bar{h}_w}=\frac{\bar{\tau}_w\cdot g}{\bar{u}} \qquad (11)$$

where $\bar{\tau}_w$ is the integrated shearing stress acting on the wall area

$$\bar{\tau}_w=\frac{1}{A_w}\int_0^{L_c}\tau_w dA_w$$

and $\bar{h}_r$ is the average value of the recovery enthalpy of the gas. The average velocity $\bar{u}$ can be taken as u_2, since the decelerating effects due to the precombustion shock and heat addition are about cancelled by the accelerating effects due to combustor divergence.[11] Defining the shear parameter as

$$\bar{C}_f=2\bar{\tau}_w/(\rho_2u_2^2) \qquad (12)$$

and noting that $\dot{w}_2=g\rho_2u_2A_2$ results in

$$\frac{\bar{C}_f}{2}=\frac{\bar{Q}/A_w}{\dot{w}_a\Delta h/A_2}\,\frac{\Delta h}{\bar{h}_r-\bar{h}_w} \qquad (13)$$

where the first right-hand term is the heat flux parameter just defined and Δh is given in Eq. (10). Whereas the simple definition of the average total enthalpy as the arithmetic mean of the combustor inlet and exit enthalpies was suitable when used to normalize the heat transfer data, a more appropriate representation is needed when defining $\bar{h}_r$ in order to obtain reasonable values of $\bar{C}_f$.

To be consistent with the usual definition of recovery enthalpy

$$\bar{h}_r\equiv C_1\bar{h}_t$$

where

$$C_1=\left[1+\bar{r}\left(\frac{\bar{\gamma}-1}{2}\right)\bar{M}^2\right]\Big/\left[1+\left(\frac{\bar{\gamma}-1}{2}\right)\bar{M}^2\right]\approx 0.93 \qquad (14)$$

for $\bar{M}$ between 2 and 4, $\bar{r}\approx(\text{Prandtl no.})^{1/3}\approx 0.9$. The average total enthalpy is defined as

$$h_t\equiv h_{t_2}+fh_{t_f}+C_2f\cdot\eta_c\cdot\Delta H_f \qquad (15)$$

In Ref. 11, the longitudinal variation of h_t was deduced from a test with hydrogen fuel to obtain a value $C_2=0.9$. For liquid fuels, the endothermic vaporization process both slows the burning and absorbs a portion of the heat released by chemical reactions and the corresponding value of C_2 is 0.4.[5] Thus, with C_2 and C_1 defined, Eqs. (12-15) can be solved which, together with the heat-transfer correlation, gives the shear parameters shown in Fig. 4 and, in turn, permits the evaluation of the shear term in Eq. (7).

The wall pressure force in Eq. (6) is taken as

$$p_wA^{\epsilon/\epsilon-1}=\text{constant}=(p_3/p_2)p_2A_2^{\epsilon/\epsilon-1} \qquad (16)$$

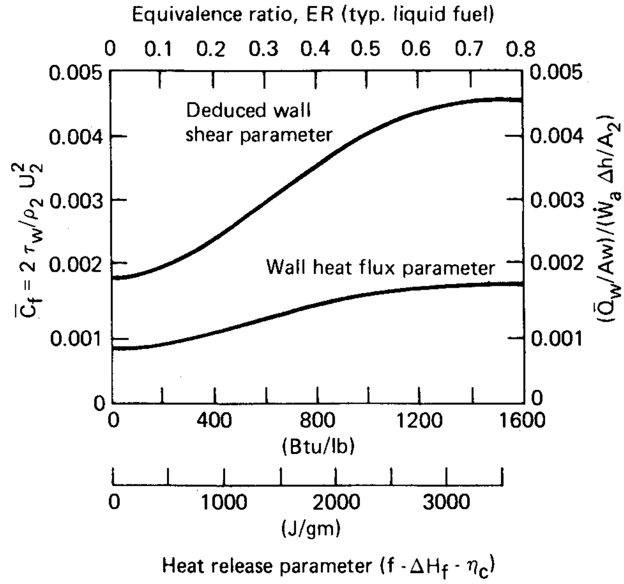

Fig. 4 Combustor wall heat transfer and skin friction coefficient as a function of equivalence ratio.

where ϵ is an arbitrary constant $-\infty \leq \epsilon \leq \infty$,[12] and

$$\int_2^4 p_w \sin\alpha \, dA_w = (1-\epsilon)[p_4 A_4 - (p_3/p_2)p_2 A_2] \quad (17)$$

Equations (6) and (8) can now be solved simultaneously for any given value of h_{t_4}. A different solution having a different value of ϵ will exist for every value of h_{t_4}. However, numerous experiments[13] have shown that the "entropy limit" condition postulated in Ref. 4 is observed. This condition is met when the value of ϵ corresponds to that given in the implicit relationship

$$\frac{\bar{\epsilon}}{\bar{\epsilon}+\gamma_4(1-\bar{\epsilon})} = \left[\frac{p_2}{p_3}\left(\frac{1}{\gamma_4}+M_2^2\right)-\left(\frac{1-\bar{\epsilon}}{\gamma_4}\right)\right]\Big/\left(\frac{A_4}{A_2}\right)^{1/(1-\epsilon)} - \frac{\bar{\epsilon}}{\gamma_4} \quad (18)$$

Note that

$$\bar{\epsilon} = \gamma M_4^2 / [1+(\gamma_4-1)\bar{M}_4^2] \quad (19)$$

and

$$0 \leq \bar{\epsilon} \leq \gamma_4/(\gamma_4-1) \quad (20)$$

When this additional constraint is added, there now is a unique solution for every ER. However, additional constraints apply for the special conditions of shock-pressure ratios, p_3/p_2, too low to separate the boundary layer at station 2, p_3/p_2 values corresponding to detached waves and p_3/p_2 larger than that corresponding to a normal shock. For these three situations, the following procedures apply. For

$$1 < (p_3/p_2)_{\epsilon=\bar{\epsilon}} < (p_3/p_2)_{\text{sep}}$$

where $(p_3/p_2)_{\text{sep}}$ can be obtained from, e.g., Ref. 14, use solutions for $p_3/p_2 = 1$, i.e., $\epsilon \neq \bar{\epsilon}$. For

$$(p_3/p_2)_{\text{det}} < (p_3/p_2)_{\epsilon=\bar{\epsilon}} < (p_3/p_2)_{\text{N.S.}}$$

where $(p_3/p_2)_{\text{det}}$ can be obtained for wedge flow from Ref. 15, use $(p_3/p_2) = (p_3/p_2) =_{\text{N.S.}}$ and $\epsilon \neq \bar{\epsilon}$. For

$$(p_3/p_2)_{\epsilon=\bar{\epsilon}} > (p_3/p_2)_{\text{N.S.}}$$

use $(p_3/p_2) = (p_3/p_2)_{\text{N.S.}}$ and $\epsilon \neq \bar{\epsilon}$ with the limit that $M_4 \geq 1$.

Cases for $M_4 < 1$ occur at low M_2 if A_4/A_2 is small and ER is large. Solutions having $M_4 < 1$ are meaningless in that the initial conditions into the combustor could not be matched by an acceptable method of inlet operation.

Nozzle

To obtain conditions at station 5, isentropic expansions are calculated for cases of specified A_5/A_4 or p_5/p_4. Two cases are computed – one assuming thermodynamic equilibrium, the other assuming a constant chemical composition "frozen" at station 4. Losses in nozzle exit stream thrust due to friction, divergence, nonuniformity, and nonequilibrium flow for all M_0's are then assumed to be accounted for in the expression

$$\mathfrak{F}_5 = \eta_n(\mathfrak{F}_{5_{\text{EQ}}} + 2\mathfrak{F}_{5_{\text{FZ}}})/3 \quad (21)$$

where $\mathfrak{F}_{5_{\text{EQ}}}$ and $\mathfrak{F}_{5_{\text{FZ}}}$ are the values of stream thrust at station 5 corresponding to equilibrium and frozen expansions, respectively. Although this appears to be a rather simplistic approach to account for losses due to chemical nonequilibrium, experimental data from freejet tests[2] at $M_0 = 5.0$, 5.8, and 7.0 have shown it to be valid when storable liquid fuels are used. Typical values of η_n are 0.97-0.98. Finally, engine gross thrust is obtained from

$$F = \mathfrak{F}_5 - \mathfrak{F}_0 - p_0(A_5 - A_0) \quad (22)$$

Optimization of a Fixed-Geometry Scramjet Engine Design

Design Requirements

With the complete engine cycle analysis thus established, it is now possible to demonstrate its utility in developing and optimizing the design of a vehicle propelled by a scramjet engine. Since optimization invariably is dependent on the mission of the vehicle under consideration, as will become apparent in the subsequent discussion, a specific mission is specified for this example. In particular, this vehicle is assumed to be a two-stage rocket-boosted scramjet missile that is to have high accelerative capabiltiy from its end-of-rocket boost $M_0 = 4$ condition at low altitude to cruise at high altitude at $M_0 = 8$ and have high lateral maneuverability. The principle consideration in the selection of a configuration is assumed to be a high thrust capability. Thrust efficiency, i.e., thrust per unit fuel flow rate is also an important parameter in configuration selection, especially if range is an important element in the mission requirement. This exemplary case, however, will only consider thrust optimization. As with most missiles, it must fit within a prescribed packaging volume, which is taken to be 21 in. (0.533 m) diam by 150 in. (3.81 m) in length. Missile cost and complexity considerations restrict the study to fixed geometry configurations.

Selection of a Configuration

Given the previous constraints and objectives, the first phase of the design study is to determine the best general class of engine design from a set of candidate configurations. Figure 5 shows schematic illustrations of three general classes of scramjet engines. Figure 5a is an all-internal contraction engine with a cylindrical "central-hole" combustor. Figure 5b is a modular engine[2] in which the captured inlet flow is subdivided into four separate ducts which traverse the entire length of the vehicle. Figure 5c is central spike design where the inlet flow is ducted to an annular combustion chamber. Lengths of each of the major engine components, viz., inlet, thru-duct combustor, and nozzle, are taken to be the same for each type of configuration. The inlet length $L_i = 32$ in. (0.813 m) and nozzle length $L_n = 22$ in. (0.559 m) were determined by the methods given in Refs. 16 and 17, respectively. The combustor length $L_C = 24$ in. (0.61 cm) is typical of several tested configurations.[3] The remaining length, which must be used to provide packaging volume for fuel, etc., becomes a thru-duct to bring the inlet air to the combustor. It has a length $L_d = 72$ in. (1.829 m).

Previous studies[18] have shown that the internal friction in a scramjet engine can be a principal cause of loss in performance. Since the three configurations have significantly different internal wetted areas, as shown on the table inset on Fig. 5, examination of the magnitude of the losses could be important in the selection of the class of configuration. To examine this issue, a single flight condition $M_0 = 6.0$ in the tropopause was examined. Calculations were made for an exit-to-inlet area ratio A_5/A_i, inlet contraction ratio A_i/A_1, and combustor exit-to-inlet area ratio A_4/A_2 of 2.0, 0.125, and 2.0, respectively, for all three configurations. The thru-duct was assumed to have a constant cross-sectional area over its entire length thus $A_2 = A_1$, and the nozzle efficiency η_n taken to be 0.975.

The resulting values of $C_t = F/q_0 A_5$ for the three engines are shown in Fig. 6. From these results, it is apparent that the modular design has significantly more thrust at the same ER than the annular design. The inlets for both configurations are primarily external compression, so inlet starting would

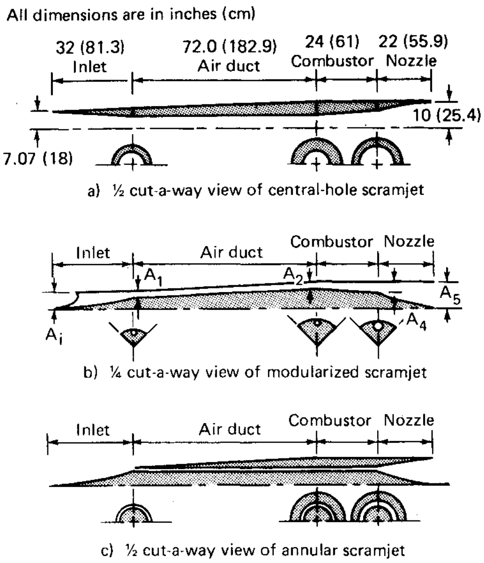

Internal wetted areas

Configuration	Air duct A_w/A_1	Combustor A_w/A_2
Central-hole	57.60	23.20
Modularized	115.20	46.37
Annular	293.48	99.71

Note: In all three cases, A_i/A_1, A_4/A_2, A_5/A_i, and component lengths are identical.

Fig. 5 Schematics of possible scramjet configurations.

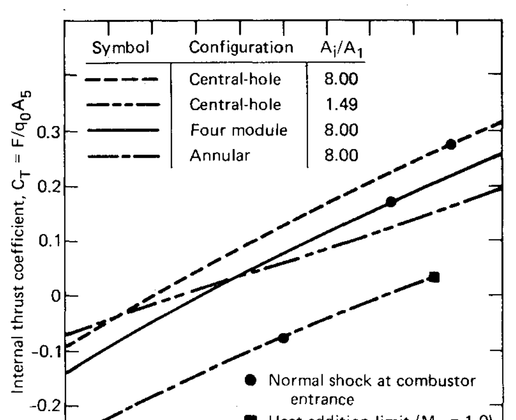

Fig. 6 Performance of candidate scramjet designs at Mach 6.

not be a problem. On the other hand, an important capability of a maneuvering vehicle is stable operation at high angles of attack. At high angles of attack, the inlet flow on the leeward side of annular inlets will separate and become unstable and either buzz or unstart once leeward separation occurs.[16] In the modularized design, on the other hand, because each module is a separate entity, if separation occurs, only the module in which it occurs will become unstable or unstart, leaving the remaining modules (three in this case) unaffected. For these reasons, the modular design is selected in favor of the annular.

Because the central-hole all-internal contraction configuration has the lowest internal wetted area, it has the highest C_T for a given ER, as shown in Fig. 6. Unfortunately, this inlet will not self-start with the contraction ratio assumed

Table 1 Maximum total temperature rise

M_0	$T_{t_0} = T_{t_2}$, °R	$T_{t_4}/T_{t_2\,\mathrm{max}}$
4	1650	3.45
5	2225	2.72
6	2930	2.25
7	3750	1.91
8	4550	1.69

and, even though a diaphragm-type arrangement could be used to initially start the inlet, self-starting after ramjet ignition in the event of flame-out is unlikely for the A_i/A_I assumed, but is highly desirable in a missile. Bleed doors are another possibility but add considerably to the complexity, cost, and lost packaging volume. If the contraction ratio A_i/A_I must be reduced from 8 to 1.48 to permit self-starting, then the performance is drastically reduced, as shown in Fig. 6. For these reasons, the all-internal contraction design was eliminated from further consideration.

Performance Optimization Procedure and Example Engine Design

Having established a general configuration to work with, i.e., the four-module design, it is now possible to apply the cycle analysis previously developed to opitmize its internal geometry in order to achieve the desired goal of maximum internal thrust in a fixed-geometry engine. To do this, there are basically three steps which need to be taken. First, since the inlet and nozzle length are fixed, a tradeoff of air duct length vs combustor length needs to be made to establish the optimum lengths of each; that is, since the total length of air duct-plus-combustor is fixed, determine the split between the two that will result in optimum performance (maximum thrust in this case). After establishing the air duct/combustor lengths, a parametric study in which all of the engine's geometric variables (other than length) are varied is needed to establish a complete matrix of engine internal performance covering the anticipated M_0/altitude flight regime. The loci of this map will then define the maximum performance possible in a completely variable geometry engine. Finally, since the ultimate goal is to design a fixed geometry engine with maximum thrust, the third step is to select a particular fixed geometry (including the design Mach number M_{des} of the inlet) for maximum average thrust over the required mission trajectory.

For the first step (air duct/combustor length selection), there are three elements to consider: the combined total pressure loss due to wall skin friction in the air duct and combustor, the minimum combustor length needed for high combustion efficiency η_c, and the minimum air duct length needed to isolate the precombustion shock/boundary-layer interaction region from the inlet. The wall skin friction coefficient in the air duct, $\bar{C}_{f_d}$, is nearly constant ($\bar{C}_{f_d} \simeq 0.0018$) but, as shown in Fig. 4, $\bar{C}_{f_c}$ increases with increasing heat release from $\bar{C}_{f_c} \simeq 0.0018$ for no heat release to $\bar{C}_{f_c} \simeq 0.0046$ at stoichiometric condition in the combustor. Consequently, for a given amount of heat release ($1 \leq T_{t_4}/T_{t_2} \leq$ stoichiometric), the combined total pressure loss due to wall friction in the air duct and combustor increases with combustor length. Moreover, for a shorter thru-duct, M_2 is higher and the pressure loss associated with the heat addition process is greater, resulting in a decrease in the combustor exit-to-air duct inlet stream thrust ratio $\mathfrak{F}_4/\mathfrak{F}_I$. However, this also decreases the combustor exit Mach number M_4, which, for a fixed area expansion nozzle, A_5/A_4, results in a larger value of nozzle exit-to-combustor exit stream thrust ratio $\mathfrak{F}_5/\mathfrak{F}_4$. Since it is the product of $\mathfrak{F}_2/\mathfrak{F}_I \times \mathfrak{F}_5/\mathfrak{F}_2$ which ultimately determines the engine's internal thrust, and the slopes of each are opposite in sign

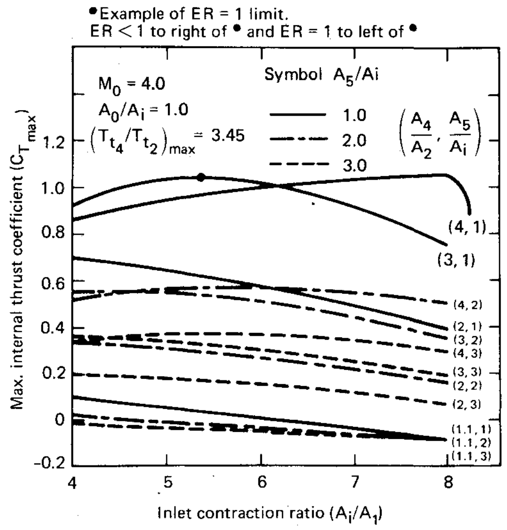

Fig. 7 Maximum internal thrust coefficient as a function of A_i/A_1, A_4/A_2, and A_5/A_i for $M_0 = 4.0$, $A_0/A_i = 1.0$.

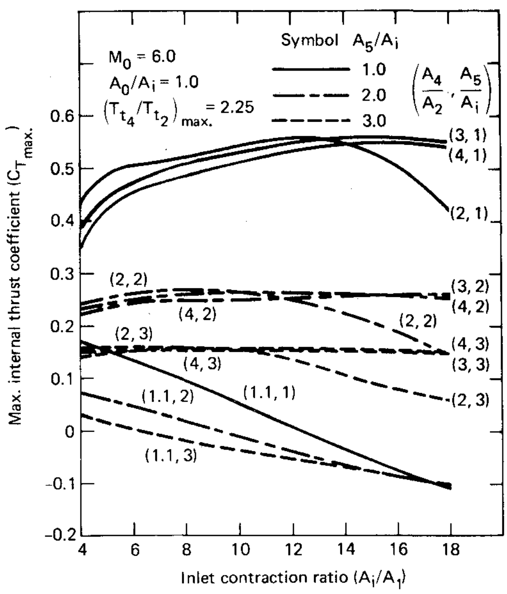

Fig. 8 Maximum internal thrust coefficient as a function of A_i/A_1, A_4/A_2, and A_5/A_i for $M_0 = 6.0$, $A_0/A_i = 1.0$.

(i.e., $\Delta(\mathfrak{F}_4/\mathfrak{F}_1)/\Delta L_c < 0$ and $\Delta(\mathfrak{F}_5/\mathfrak{F}_4)/\Delta L_c > 0$), previous studies[19] have shown that for the high value $(L_d + L_c)/D_d$ of this configuration, increasing L_c may actually increase engine thrust slightly. However, since calculations for $L_c = 18$ in. (46 cm) to 48 in. (122 cm) showed only a $\pm 3\%$ difference for $L_d + L_c = 96$ in. (2.44 m), $L_c = 24$ in. (61.0 cm) has been assumed for the remainder of this study, which is close to the minimum length needed to achieve nearly complete combustion of highly reactive liquid fuels,[2] thus leaving a $L_d = 72$ in. (1.83 m), which is more than adequate to prevent combustor-inlet interactions.[13]

With the lengths of each of the components established, it is now possible to generate a complete matrix of engine internal performance wherein M_0 and all geometric areas are varied over a suitable range of values. Since the engine is intended for $M_0 = 4$-8 flight, engine internal thrust coefficients, $C_T = F/q_0A_5$, have been calculated for $M_0 = 4$, 6, and 8 flight within the tropopause. To minimize the cost of this large number of calculations, $\gamma = 1.4$ throughout the cycle was assumed and heat transfer to the walls was assumed negligible. Also, the keep the results as general as possible rather than restricting the results to a specific fuel, an

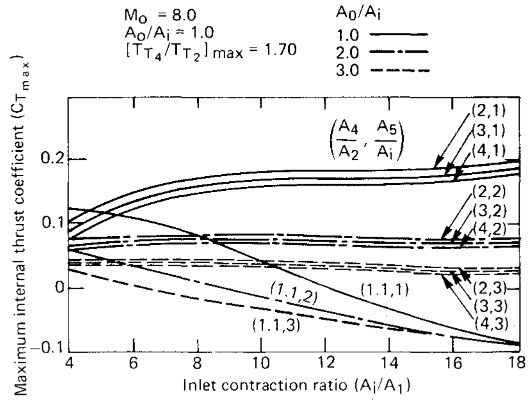

Fig. 9 Maximum internal thrust coefficient as a function of A_i/A_1, A_4/A_2, and A_5/A_i for $M_0 = 8$, $A_0/A_i = 1.0$.

analytical expression[20] relating combustor total temperature rise T_{t_4}/T_{t_2} to fuel-air equivalence ratio ER and freestream total temperature T_{t_0} has been used, viz.,

$$(T_{t_4}/T_{t_2}) = 1 + \mathrm{ER}[(4500/T_{t_2}) - 0.3] \tag{23}$$

For flight within the tropopause, the maximum T_{t_4}/T_{t_2} (@ER = 1) for a given flight Mach number, assuming $\eta_c = 1.0$, is shown in Table 1.

$\bar{C}_{f_c}$ is also a function of T_{t_4}/T_{t_2} and an analytical expression is used to represent it in the theoretical calculations. Again, for simplicity, a linear approximation

$$\bar{C}_{f_c} = 0.0018 + 0.0028[(T_{t_4}/T_{t_2}) - 1]/[(T_{t_4}/T_{t_2})_{\max.} - 1] \tag{24}$$

is used to represent the curve shown in Fig. 4.

In addition, it is assumed for clarity that there are no changes in effective internal areas due to boundary-layer growth, i.e., in the air duct, combustor and nozzle. Effective changes in the area of the inlet's throat are accounted for in the geometric inlet contraction ratio, A_i/A_1, used.

With these assumptions established, C_T's were calculated for a variety of internal area ratios and the resulting maximum values of $C_{T_{\max}}$ for a given geometry plotted in Figs. 7-9 for $M_0 = 4$, 6, and 8. In each case, $A_0/A_i = 1.0$ and A_5/A_i was varied between 1.0 and 3.0, A_i/A_1 between 4 and 18 (where possible), and A_4/A_2 between 1.1 and 4.0. Note that when A_5/A_i increases, A_i decreases, since A_5 is fixed. In all cases, it was assumed that the inlet's kinetic energy efficiency η_{KE} varied linearly between 0.98 at $M_0 = 4$ to 0.95 at $M_0 = 8$ regardless of the value of A_i/A_1 assumed. Generally, η_{KE} would decrease slightly with increasing A_i/A_1, but with the previously expressed intent for simplicity, this effect was ignored.

For all three M_0's, $C_{T_{\max}}$ occurs when $A_5/A_i = 1$, but at different A_i/A_1's and A_4/A_2's. Thus, cases having $A_5/A_i > 1$ will not be discussed. On the other hand, to understand or interpret the character of the curves for $A_5/A_i = 1$, it is necessary to discuss the ramifications of inlet design on the operating limits of the combustor. Unlike a conventional ramjet, where the throat of an external compression inlet (with perhaps some internal contraction) is, in general, sized to keep the inlet in its supercritical mode at all operating conditions, the throat of a scramjet inlet must be sized to maintain M_2 high enough to permit sufficient heat to be added to produce a reasonable net thrust coefficient $(C_T - C_D)$ at the lower M_0's. An illustrative example of this is shown in Figs. 10 and 11 for $M_0 = 4$ and 6, A_5/A_i and $A_4/A_2 = 2.0$. Figure 10 presents C_T vs ER for $A_0/A_i = 0.6$, 0.8, and 1.0 and $A_i/A_1 = 4$ and 8, and Fig. 11 presents the corresponding values of M_2 vs A_i/A_1 for $A_0/A_i = 0.6$, 0.8, and 1.0. Referring to Fig. 10, three things are apparent. First,

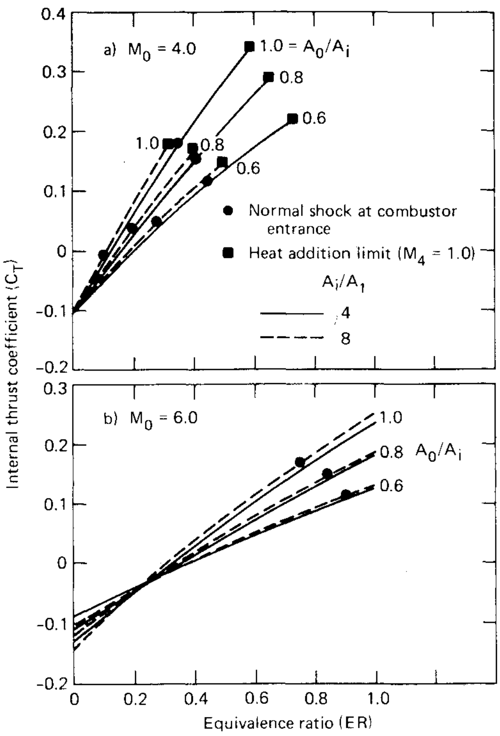

Fig. 10 Internal thrust coefficient as a function of equivalence ratio, A_i/A_1, and A_0/A_i for $M_0 = 4$ and 6.0, $A_4/A_2 = 2.0$, $A_5/A_i = 2.0$.

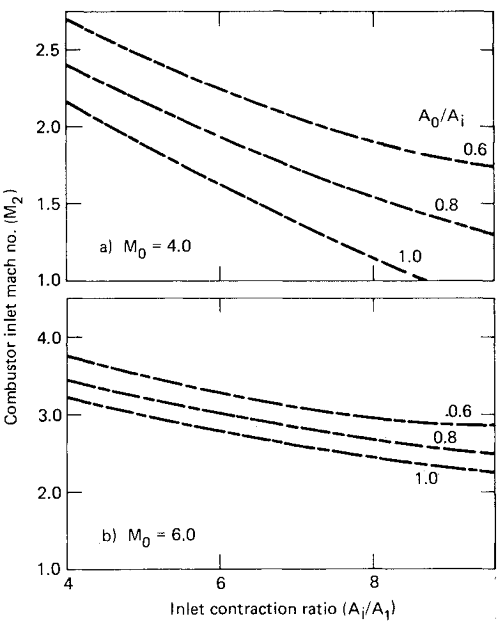

Fig. 11 Combustor inlet Mach number as a function of A_i/A_1 and A_0/A_i for $M_0 = 4$ and 6, $A_4/A_2 = 2.0$, $A_5/A_i = 2.0$

at $M_0 = 4$ (Fig. 10a), combustion at the higher ER's is in all cases preceded by a normal shock (to the right of the dark circles), i.e., combustion being in a subsonic flow but the axial pressure gradient accelerates the flow to supersonic conditions prior to the combustor exit (sometimes referred to as dual-mode combustion). For $A_0/A_i = 1.0$, dual-mode combustion occurs over the range $0.36 \leq ER \leq 0.59$ for $A_i/A_1 = 4$ and over the range $0.11 \leq ER \leq 0.31$ for $A_i/A_1 = 8$. For ER values to the left of the dark circles, combustion is preceded by an oblique shock and the flow through the combustor is entirely supersonic. As the Mach number M_0 increases, the ER at which the combustion is preceded by a normal shock increases (Fig. 10b vs Fig. 10a). In general, for

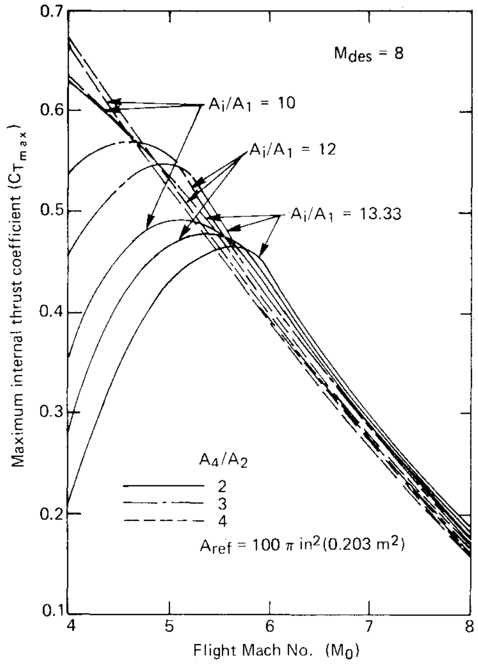

Fig. 12 Maximum internal thrust coefficient as a function of M_0 for $A_5/A_i = 1.0$, $A_4/A_2 = 2$, 3, and 4.

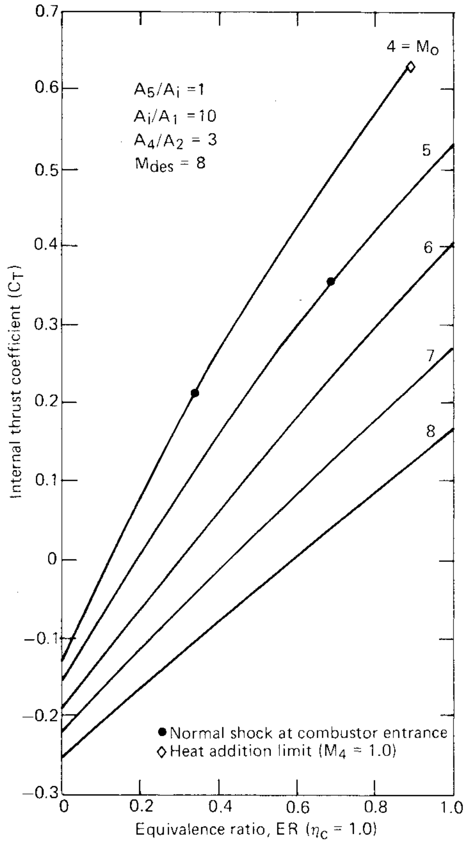

Fig. 13 Internal thrust coefficient as a function of equivalence ratio and M_0 for optimized four-module scramjet engine.

$M_0 \gtrsim 6.5$, stoichiometric (ER = 1) heat release can be obtained without the presence of a normal shock. The equivalence ratio corresponding to the maximum permissible heat release, $ER_{max.}$, also increases with decreasing A_0/A_i or A_i/A_1 at a fixed M_0 and increases with M_0 at a fixed A_0/A_i. The $ER_{max.}$ values are indicated by the dark squares ($M_4 = 1$) in Fig. 10a. For $A_0/A_i = 1.0$ and $A_i/A_1 = 4$, $ER_{max.} = 0.59$ and for

$A_i/A_l = 8$, $ER_{max.} = 0.31$. Since $ER_{max.}$ decreases rapidly with increasing A_i/A_l, the corresponding values of C_T also decrease. The cases where $ER_{max.}$ is limiting have relatively low values of M_2, i.e., at $M_0 = 4$, $A_0/A_i = 1$, $M_2 = 2.15$ for $A_i/A_l = 4$ and $M_2 =$ for 1.16 for $A_i/A_l = 8$, and $M_2 = 1$ ($ER_{max.} = 0$) at $A_i/A_l \simeq 8.7$, as shown in Fig. 11a. Although not shown, at $M_0 = 5$ with higher values of A_i/A_l, $ER_{max.} < 1$ but at $M_0 = 6$, full stoichiometric heat release can be obtained at the values of A_0/A_i shown without reaching $M_4 = 1$, as shown in Fig. 11b. Decreasing A_0/A_i alleviates these limits, since the freestream air is contracted through a smaller effective area, $(A_i/A_l)_{eff} = A_i/A_l \times A_0/A_i$, resulting in a higher M_2 (Fig. 11), but with a corresponding decrease in $C_{T_{max.}}$ (Fig. 10). It should be noted that decreasing A_4/A_2 from the nominal value of 2.0 used in Figs. 10 and 11 will lower the ER at which the normal shock and thermal choking occur at a given M_0 and vice versa when it is increased. Finally, the maximum C_T will occur at the maximum inlet air capture ratio, i.e., $A_0/A_i = 1.0$ since the effect of increasing engine airflow which gives higher C_T for a given ER as illustrated in Fig. 10 more than overcomes the $M_4 = 1$ limit.

Returning now to Figs. 7-9, it is possible to explain the trends shown in the curves for $A_5/A_i = 1$ (solid curves). In general, for a fixed A_4/A_2, $C_{T_{max.}}$ will monotonically increase with increasing A_i/A_l as long as the $M_4 = 1$ limit does not restrict the ER to be less than stoichiometric. From the point where $M_4 = 1$ and $ER = 1$, $C_{T_{max.}}$ will monotonically decrease with increasing A_i/A_l. The condition where $M_4 = 1$, $ER = 1$ is indicated by a solid circle on the $A_4/A_2 = 3$, $A_5/A_i = 1$ curve in Fig. 7. Furthermore, the $A_4/A_2 = 2$, $A_5/A_i = 1$ curve in this figure corresponds to a locus of points all having $ER < 1$. Conversely, from Fig. 8, the curves for $A_4/A_2 = 3$, $A_5/A_i = 1$ and $A_4/A_2 = 4$, $A_5/A_i = 1$ represent points all having $ER = 1$.

From Fig. 7 at $M_0 = 4$, it is apparent that the highest value of $C_{T_{max.}}$ would lie between A_4/A_2 values of 3 and 4, say at $A_4/A_2 \sim 3.5$, $A_i/A_l \sim 6$. At $M_0 = 6$, $C_{T_{max.}}$ would be essentially on the $A_4/A_2 = 2$ curve at about $A_i/A_l = 13$ (Fig. 8) and at $M_0 = 8$, $C_{T_{max.}}$ is at $A_4/A_2 = 2$ and $A_i/A_l = 18$. Since the purpose is to select one geometry that will result in the best overall $C_{T_{max.}}$, some compromise must be made in the selection of A_4/A_2 and A_i/A_l. Fortunately, one factor that has not yet entered the discussion, viz., inlet air capture at $M_0 < M_{des}$, tends to reduce the range of inlet contraction ratios that need to be considered. By selecting an inlet design Mach number equal to the highest operating M_0, the effective contraction ratio of a fixed geometry inlet is reduced at $M_0 < M_{des}$, which permits the selection of a larger A_i/A_l than would have been permitted at low M_0. To exemplify this point and to enable the selection of the A_i/A_l, it will be assumed that $M_{des} = 8$ and that A_0/A_i varies linearly between 0.6 at $M_0 = 4$ to 1.0 at $M_0 = 8$, which is not atypical of a fixed geometry scramjet inlet.[2] Figure 7 shows that contraction ratios greater than about 8 would result in low values of $C_{T_{max.}}$ for $M_{des} = 4$. However, if $M_{des} = 8$, then the servere drop in C_T would not occur until $(A_i/A_l)_{eff} = 8 \div 0.6 = 13.33$. Thus, the range of interest of A_i/A_l extends from about $6 \div 0.6 = 10$ to about 13.33.

Figure 12 shows $C_{T_{max.}}$ for $A_4/A_2 = 2$, 3, and 4 cross-plotted vs M_0 for three values of A_i/A_l covering the range of interest for an $M_{des} = 8$ engine. Although several different criteria could be used to select A_4/A_2 and A_i/A_l, the one chosen herein is simply the highest average $C_{T_{max.}}$ for $M_0 = 4$-8, which can be found by integrating the area under the curves. When this is done, it results in $A_i/A_l = 10$, $A_4/A_2 = 3$ being the optimum fixed geometry four-module scramjet configuration. To complete the procedure, engine C_T as a function of ER for $M_0 = 4$-8 is presented in Fig. 13. Note that the maximum ER at $M_0 = 4$ is 0.84 and for $M_0 > 5.5$ the engine operates over the entire ER range in the all-supersonic mode.

Having selected an engine geometry and obtained the predicted thrust coefficients, it is necessary to reconsider the mission requirements, i.e., typical trajectories are determined and the overall performance of the engine over the entire trajectory is obtained. On occasion, this could result in a redefinition of the engine geometry. For example, it could be found that the engine had inadequate thrust to accelerate and climb from a low M_0, say $M_0 = 4$ in the previous example. To solve this problem, A_4/A_2 could be increased to 4 (Fig. 12) to obtain about 20% greater accelerative capability, but with a corresponding loss in $C_{T_{max.}}$ at high M_0. On the other hand, it may be found that adequate thrust is available at all flight conditions and, therefore, a smaller inlet could be considered which would reduce missile weight and could increase specific impulse. Moreover, considerations of the effects of engine geometry or aerodynamics, structure, internal stowage (guidance, fuel, etc.), and booster sizing must be included in any system optimization study. They have not be included here, since the purpose of this paper was to outline the methodology for optimizing the propulsive design of a scramjet-powered vehicle using the engine cycle analysis presented in the first part of the paper.

Concluding Remarks

A complete supersonic combustion ramjet (scramjet) engine cycle analysis has been presented. The methodology for applying this cycle analysis to optimizing the engine design of a scramjet-powered missile has also been presented along with a specific numerical example. The latter illustrates the special considerations in engine geometry that are needed to produce a viable scramjet engine.

Acknowledgment

This work was supported by the U.S. Navy (VAVSEA-03) under Contract NAVSEASYSCOM N00024-78-C-5384.

References

[1] Weber, R.J. and MacKay, J.S., "An Analysis of Ramjet Engines Using Supersonic Combustion," NACA TN 4386, Sept. 1958.

[2] Waltrup, P.J., Anderson, G.Y., and Stull, F.D., "Supersonic Combustion Ramjet (SCRAMJET) Engine Development in the United States," *The 3rd International Symposium of Air Breathing Engines*, The Johns Hopkins University Applied Physics Laboratory Preprint 76-042, March 1976.

[3] Billig, F.S., Orth, R.C., and Funk, J.A., "Direct-Connect Tests of a Hydrogen-Fueled Supersonic Combustor," NASA CR-1904, Aug. 1971.

[4] Billig, F.S. and Dugger, G.L., "The Interaction of Shock Waves and Heat Addition in the Design of Supersonic Combustors," *Twelfth Symposium (International) on Combustion*, The Combustion Institue, Pittsburgh, Pa., 1969, pp. 1125-1134.

[5] Orth, R.C., Billig, F.S., and Grenleski, S.E., "Measurement Techniques for Supersonic Combustor Testing," *AIAA Progress in Astronautics and Aeronautics*, Vol. 34, MIT Press, 1974.

[6] Midgal, D., Hammer, S., and Agosta, V., "Scramjet Combustor and Nozzles Analysis for Two Phase Flow," PSI Rept. 68-1, Propulsion Sciences, Inc., Melville, N.Y., Jan. 1968.

[7] Fehlner, L.F. and Nice E.V., "Tabulation of Standard Atmospheres at 100-Foot Intervals of Altitude," APL/JHU TG 313-1, Aug. 1968.

[8] Perini, L.L., "Curve Fits of JANAF Thermochemical Data," APL/JHU ANSP-M-5, Sept. 1972.

[9] Cruise, D.R., "Notes on the Rapid Computation of Chemical Equilibria," *Journal of Physical Chemistry*, Vol. 68, 1964, p. 3797.

[10] Billig, F.S., "Heat Transfer Processes in Supersonic Combustion," to be published.

[11] Billig, F.S. and Grenleski, S.E., "Experiments and Analysis of Heat Transfer in Supersonic Combustion Processes," *Fourth International Heat Transfer Conference*, Paris, Versailles, Aug. 1970, Vol. 3, Elsevier Publishing Company, Amsterdam, 1970.

[12] Billig, F.S., "Design of Supersonic Combustors Based on Pressure-Area Fields," *Eleventh Symposium (International) on Combustion,* The Combustion Institute, Pittsburgh, Pa., 1967, pp. 755-759.

[13] Waltrup, P.J. and Billig, F.S., "Prediction of Precombustion Wall Pressure Distributions in Scramjet Engines," *Journal of Spacecraft and Rockets,* Vol. 10, Sept. 1973, pp. 620-622.

[14] Mager, A., "On the Model of the Free, Shock-Separated Turbulent Boundary Layer," *Journal of Aeronautical Sciences,* Vol. 23, Feb. 1956, p. 181.

[15] "Equations, Tables, and Charts for Compressible Flow," NACA Rept. 1135, 1953.

[16] Faro, I.D.V. and Keirsey, J.L., "Supersonic Inlets," in *Ramjet Technology,* Applied Physics Laboratory/Johns Hopkins University TG-610-3B, Nov. 1967, Chap. 3B.

[17] Agosta, V. and Hammer, S., "Scramjet Nozzle Analysis," PSI Rept. 70-1, Propulsion Sciences, Inc., Melville, N.Y., Feb. 1970.

[18] Waltrup, P.J., Dugger, G.L., Billig, F.S., and Orth, R.C., "Direct-Connect Tests of Hydrogen-Fueled Supersonic Combustors," *XVIth International Symposium on Combustion,* The Combustion Institute, Pittsburgh, Pa., 1977, pp. 1619-1629.

[19] Waltrup, P.J., "Combustor/Through-Duct Length Variations in a Fixed Length Hypersonic Engine," Sec. 40, *Research and Development Programs Quarterly Report,* U-RQR/75-2, April-June 1975, July 1975.

[20] Dugger, G.L. and Billig, F.S., "Hypersonic Ramjets," in *Ramjet Technology,* Applied Physics Laboratory/Johns Hopkins University TG-610-11, March 1970, Chap. 11.